ЖЭТФ, 2012, том 142, вып. 4 (10), стр. 797–816

PRESSURE AND TEMPERATURE INDUCED TRANSFORMATIONS IN CRYSTALLINE POLYMERS OF C_{60}

K. P. Meletov [a*], ***G. A. Kourouklis*** [b]

[a] *Institute of Solid State Physics, Russian Academy of Sciences*
142432, Chernogolovka, Moscow Region, Russia

[b] *Physics Division, School of Technology, Aristotle University of Thessaloniki*
GR-54006, Thessaloniki, Greece

Received June 23, 2011

The great advantage of the C_{60} molecule is its potential for polymerization, due to which the molecule can be the building block of new all carbon materials. In addition, it contains both sp^2 and sp^3 hybridized carbon atoms, which allows synthesizing new carbon materials with desired physicochemical properties using both types of carbon bonding. The one- and two-dimensional polymeric phases of C_{60} are prototype materials of this sort. Their properties, especially polymerization under pressure and room temperature via covalent bonding between molecules belonging to adjacent polymeric chains or polymeric layers, can be used for further development of new materials. The present review focuses on the study of the pressure-induced polymerization and thermodynamic stability of these materials and their recovered new phases by *in-situ* high-pressure Raman and X-ray diffraction studies. The phonon spectra show that the fullerene molecular cage in the high-pressure phases is preserved, while these polymers decompose under heat treatment into the initial fullerene C_{60} monomer.

Contents

1. Introduction 797

2. Pressure-induced transformations in the 2*D*-T polymer 799

3. Transformations of the 2*D*-R polymer at high pressure 805

4. Pressure- and photo-induced transformations in the linear polymer of C_{60} 809

5. Thermal stability of fullerene polymers 812

6. Conclusions 814

References 815

1. INTRODUCTION

Fullerene C_{60} is a molecular crystal formed by all-carbon molecules with a closed-cage structure and a nearly spherical shape. The molecular cages can be thought as generated by 12 pentagons and 20 hexagons with 60 equivalent carbon atoms arranged on a nearly spherical shell approximately 7 Å in diameter. Kroto et al. identified the fullerene C_{60} as an all-carbon closed-cage molecule in 1985 [1] (Nobel Prize in chemistry in 1996). At room temperature, the almost completely freely rotating C_{60} molecules form a close-packed face-centered cubic (FCC) structure. The polymerization potential of C_{60} was recognized very early as effected by the destruction of a number of double bonds and the creation of covalent bonds via [2+2] cyclo-addition reaction resulting from the sp^3-like fourfold coordinated carbon atoms. The pristine C_{60} has a great potential to form various polymeric forms due to the 30 unsaturated double C=C bonds

*E-mail: mele@issp.ac.ru

in the molecular cage. Initiators of the polymerization process have been identified as i) visible light [2], ii) alkali metal doping [3, 4], and iii) high-pressure/high-temperature (HPHT) treatment of the pristine C_{60} [5–7]. The important alterations in the structural features of the polymeric C_{60} are the decrease in the intermolecular distances and the deformation of the fullerene molecular cage, which results in lowering the symmetry of the parent C_{60} molecule [2]. The photopolymerized C_{60} material mainly contains dimers on the surface of the samples due to the small penetration depth of the visible light; the material becomes insoluble in commonly used solvents, but reverts to the initial monomer under heating for a short period of time at about 500 K [2].

Bulk quantities of C_{60} polymers have been made available after the development of the HPHT polymerization technology [5–7]. The C_{60} molecules form ordered linear polymeric chains or two-dimensional polymeric layers at low and intermediate pressure P and temperature T [5, 7]. At higher P and T, rather disordered FCC structures are formed, which are based on $3D$ cross-linked polymerization in the material [8, 9]. At high nonuniform pressure and high temperature, the disordered $3D$ polymeric phases — so-called ultrahard fullerite phases — are formed [10–13]. The linear polymeric chains ($1D$ polymer) with four sp^3-like coordinated carbon atoms in the fullerene molecular cage are obtained for temperatures in the range 500–600 K and pressure higher than 1 GPa [7]. Parallel straight chains form two orthorhombic structures that belong to the pseudo-tetragonal $Immm$ space group (pressure above 2–3 GPa) and the orthorhombic (O) $Pmnn$ space group (pressure below 2 GPa) [14].

The planar polymeric layers ($2D$ polymer) with eight or twelve sp^3-like coordinated carbon atoms in the fullerene molecular cage, obtained at temperatures in the range 700–900 K and pressures 1.5–9 GPa, form tetragonal (T) and rhombohedral (R) crystalline polymeric structures [5, 7]. The tetragonal structure, usually observed at pressures below 5 GPa, can be stabilized in two types of stacking; the $Immm$ orthorhombic structure (actually tetragonal because the a and b axes are almost equal) and the $P\,4_2/mmc$ tetragonal structure [14]. The calculated lattice energies of these structures are very close, but the energy of the $P\,4_2/mmc$ stacking is lower than that of the $Immm$ stacking, a fact that results in the growth of samples mostly containing the $P\,4_2/mmc$ structure with some inclusions of the $Immm$ structure [15]. The rhombohedral structure, usually obtained at pressures higher than 5 GPa, is also stabilized in two types of layer stacking while both structures are described by the $R\bar{3}m$ space group [14].

The interest in the polymeric structures of C_{60} arises primarily from the theoretically predicted high hardness of the $3D$ cross-linked fullerene polymers [16]. The rather disordered crystal structure of these polymers is FCC; it becomes more and more disordered as the treatment temperature is increased [14]. Theoretical investigation [17] has predicted that the ordered $3D$-polymerized C_{60} might be formed even at room temperature by the application of uniaxial pressure perpendicular to the polymeric layers of the $2D$-T phase of C_{60} belonging to the pseudo-tetragonal $Immm$ space group. According to the density functional calculations, polymerization must take effect at the lattice constant $c = 10.7$ Å, which is attainable at $P \approx 20.2$ GPa. This phase, having 24 sp^3-like and 36 sp^2-like hybridized carbon atoms per each C_{60} molecule, is stable under ambient pressure [17]. The electronic structure of the new phase is metallic, in contrast to other fullerene polymers and pristine fullerene, which are all known to be semiconducting [18, 19]. It is interesting that the calculated bulk modulus of this phase is approximately 47 GPa, which is considerably smaller than that of diamond, in contrast with the expected high stiffness of the $3D$-polymerized fullerenes [16].

Another theoretical study [20] predicted that uniaxial compression perpendicular to the chains in the $1D$ or to the polymeric layers in the $2D$ polymeric phases of C_{60} also leads to $3D$ polymerization of C_{60}. The *ab initio* calculations performed using a numerical-atomic-orbital density functional method for $1D$ and $2D$ polymeric body-centered orthorhombic C_{60} structures have shown two metastable $3D$ polymeric structures having 52 and 56 sp^3-like coordinated carbon atoms per C_{60} molecular cage. In these phases, the molecular cages are preserved, as are the polymeric bonds originally present in the chains or planes. In addition, the polymeric structure with 56 sp^3-like coordinated carbon atoms per C_{60} molecule transforms under further compression to 14 GPa to a new polymeric phase with 60 sp^3-like coordinated carbon atoms [20]. All these phases are semiconducting and their bulk and shear moduli are expected to be respectively around 300 and 260 GPa.

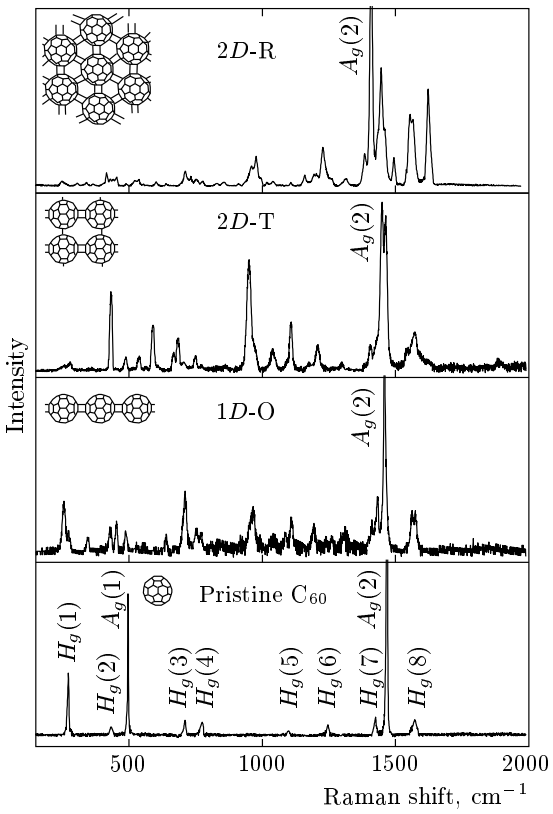

Fig. 1. Raman spectra of various polymer phases of C_{60} along with that of monomer C_{60} recorded at normal conditions. The assignment given for C_{60} refers to its molecular modes. Insets: the location of fullerene molecular cages in various polymer phases and the arrangement of intercage covalent bonds

The characterization of the crystalline polymers of C_{60} is based mainly on the X-ray diffraction studies of their crystal structure and arrangement of polymeric bonds. The important information about polymer properties can also be obtained from Raman scattering and IR-absorption optical measurements. The Raman scattering and X-ray diffraction studies can be used effectively for *in-situ* studies of phase transitions and irreversible transformations at high pressure by the use of diamond anvil cells. In addition, Raman spectroscopy applied to the pristine C_{60}, $1D$-O, $2D$-R, and $2D$-T polymers provide an effective tool for their identification. This methodology has been established through combined Raman and IR-absorption spectroscopic measurements and X-ray diffraction studies on samples prepared under carefully controlled P/T conditions [21].

Morover, the perturbations of C_{60} cages, caused by high pressure or chemical bond formation, are effectively monitored by Raman spectroscopy [22, 23]. The Raman spectra of the crystalline polymers along with that of the pristine C_{60}, emphasizing their characteristic features related to the particular material, are reproduced in Fig. 1 at ambient conditions and in the frequency region 150–2000 cm^{-1}. The insets in Fig. 1 show the location of fullerene molecular cages in the various polymeric phases and the arrangement of the intercage covalent bonds among the polymeric networks. The most important probe of the polymeric phases of C_{60} is the behavior of the $A_g(2)$ pentagonal pinch (PP) mode of the C_{60} molecule. This mode is related to the in-phase stretching vibration, which involves tangential displacements of carbon atoms with a contraction of pentagonal rings and an expansion of hexagonal rings. The PP mode frequency downshifts in all polymeric forms of C_{60} due to the formation of the intermolecular covalent bonds. This leads to a decrease in the average intramolecular bond stiffness.

In the case of the FCC crystal structure of the C_{60} monomer, the $A_g(2)$ mode is observed at 1468 cm^{-1}. In the $1D$-O polymer, this mode is observed at 1458 cm^{-1} [21]. In the $2D$-T polymer, two intense peaks at 1446 and 1464 cm^{-1} are observed; the peak at 1446 cm^{-1} has been proposed to be the PP mode of the $2D$-T polymer and the 1464 cm^{-1} peak may be attributed to the presence of C_{60} dimers or activation of the $\{F_{1g}(3)\}$ molecular mode [21]. Finally, in the case of the $2D$-R phase, the $A_g(2)$ mode exhibits the strongest softening and is observed at 1408 cm^{-1}. The phonon frequencies of the crystalline polymeric phases of C_{60} and the mode assignment, based on the icosahedral symmetry of the parent C_{60} molecule [21, 24, 25], are tabulated in Table 1.

In this review, we discuss the experimental studies of pressure-induced transformations in the linear and planar crystalline polymeric phases of C_{60}. We present the systematic work related to the linear and planar polymers of C_{60} with the intention to document the pressure-induced transformations associated with the increase in the degree of polymerization. We believe that starting with the polymerization process of C_{60}, additional materials interesting for applications will be produced involving both carbon bond properties and various forms of dimensionality. This becomes more appealing after the new insight into carbon materials has been provided by the graphene structure properties.

2. PRESSURE-INDUCED TRANSFORMATIONS IN THE $2D$-T POLYMER

For some important reasons, we begin with the $2D$-T polymer. This polymeric form has a structure

Table 1. Phonon frequencies for the $2D$-R, $2D$-T, $1D$-O, and the transformed $1D$-O polymer phase of C_{60}. The corresponding values for monomer C_{60} are also included

$2D$-R polymer [30]		$2D$-T polymer [26]		$1D$-O transformed [47]		$1D$-O polymer [47]		Monomer C_{60} [21]	
Mode	ω_i, cm^{-1}	Mode	ω_i, cm^{-1}	Mode*	ω_i, cm^{-1}	Mode	ω_i, cm^{-1}	Mode	ω_i, cm^{-1}
$H_g(1)$	245	$H_g(1)$	259		248	$H_g(1)$	251	$H_g(1)$	273
$H_g(1)$	267	$H_g(1)$	280		266	$H_g(1)$	270		
$H_g(1)$	308				288				
$H_u(1)$	342				333	$H_u(1)$	340		
$F_{2u}(1)$	366				366				
					389				
$G_u(1)$	406								
$H_g(2)$	415				411				
$H_g(2)$	438	$H_g(2)$	431		427	$H_g(2)$	425	$H_g(2)$	437
$H_g(2)$	451					$H_g(2)$	450		
$A_g(1)$	492	$A_g(1)$	481		484	$A_g(1)$	486	$A_g(1)$	496
$F_{1u}(1)$	520				521	$\Omega(x)$	523		
$F_{2g}(1)$	532	$F_{2g}(1)$	536		527				
$F_{1g}(1)$	558	$F_{1g}(1)$	563		561				
$H_u(2)$	579	$F_{1g}(1)$	588						
$H_u(2)$	596				598				
		$\Omega(x)$**	610		614				
$H_u(3)$	640				634	$H_g(3)$	635		
					654				
		$H_g(3)$	666		662				
$H_g(3)$	695				694				
$F_{2u}(2)$	709				707	$H_g(3)$	707	$H_g(3)$	710
$H_g(3)$	712				722				
$H_g(3)$	731				739				
$H_g(4)$	749	$H_g(4)$	747		752	$H_g(4)$	752		
$F_{2g}(2)$	767								
$H_g(4)$	776	$H_g(4)$	772		774	$H_g(4)$	769	$H_g(4)$	774
$F_{2u}(3)$	827								
$H_u(4)$	856				853	$\Omega(x)$	843		
$H_u(4)$	868	$\Omega(x)$	864						
					903	$\Omega(x)$	897		

Table 1

2D-R polymer [30]		2D-T polymer [26]		1D-O transformed [47]		1D-O polymer [47]		Monomer C_{60} [21]	
Mode	ω_i, cm^{-1}	Mode	ω_i, cm^{-1}	Mode*	ω_i, cm^{-1}	Mode	ω_i, cm^{-1}	Mode	ω_i, cm^{-1}
$G_g(2)$	958	$G_g(2)$	951		947	$\Omega(x)$	957		
					959				
$F_{1g}(2)$	977	$F_{1g}(2)$	970		969				
					987				
$F_{2u}(4)$	1016								
$F_{2u}(4)$	1037				1027	$\Omega(x)$	1034		
$H_g(5)$	1042	$\Omega(x)$	1041						
$H_g(5)$	1078	$H_g(5)$	1090		1082	$H_g(5)$	1082		
$H_g(5)$	1109	$H_g(5)$	1107		1105	$H_g(5)$	1105	$H_g(5)$	1100
$G_g(3)$	1158	$G_g(3)$	1176						
$G_g(3)$	1195				1190	$H_g(5)$	1190		
$F_{2g}(3)$	1204	$F_{2g}(3)$	1206		1205				
$H_g(6)$	1224								
$H_g(6)$	1230				1241	$H_g(6)$	1240	$H_g(6)$	1243
$H_g(6)$	1260				1257	$H_g(6)$	1258		
$G_g(4)$	1314	$G_g(4)$	1299			$H_g(6)$	1307		
$H_g(7)$	1385	$H_g(7)$	1404		1386	$H_g(7)$	1398		
$A_g(2)$	1410				1423	$H_g(7)$	1416		
		$H_g(7)$	1428		1429	$H_g(7)$	1430	$H_g(7)$	1428
		$A_g(2)$	1447		1442	$H_g(7)$	1442		
		$F_{1g}(3)$	1463		1455	$A_g(2)$	1457	$A_g(2)$	1470
$F_{1g}(3)$	1495								
$H_g(8)$	1554	$F_{2g}(4)$	1543		1559				
$H_g(8)$	1563	$H_g(8)$	1567		1559	$H_g(8)$	1560		
$H_g(8)$	1569	$G_g(6)$	1598			$H_g(8)$	1575	$H_g(8)$	1575
$G_g(6)$	1621				1621	$H_g(8)$	1621		
$G_g(6)$	1627								

*No assignment can be made. ** Some modes with unknown assignment.

belonging to the pseudo-tetragonal $Immm$ space group and provides a more straightforward way for structural transformation at high pressure as predicted theoretically [17]. In addition, the calculated new high-pressure phase has very interesting physical properties [17]. The first *in-situ* Raman measurements in the $2D$-T polymer as a function of pressure up to 12 GPa have shown a continuous and reversible pressure dependence of the phonon frequencies [26].

Further measurements at higher pressures have revealed dramatic changes in the Raman spectra, which occur in a narrow pressure region near 20 GPa [27, 28]. This is depicted in the Raman spectra of the $2D$-T polymer of C_{60} in the frequency range 180–2050 cm^{-1}, recorded for pressures up to 27.5 GPa and room temperature (Fig. 2*a*) [27]. The spectral region near the T_{2g} mode of diamond (1332 cm^{-1} at ambient pressure [29]) is omitted. As the pressure increases, the Raman peaks shift to higher energies and their bandwidth gradually increases. The broadening is further enhanced for pressures higher than 10 GPa due to the solidification of the pressure-transmitting medium. Precursors of the incoming structural transformation can be recognized as an increase in the Raman bandwidths combined with a decrease in their intensity, as well as the appearance of a new peak at a higher energy in the Raman spectrum at 17.5 GPa. Pronounced changes in the Raman spectrum are observed at the pressure 20.7 GPa; some peaks disappear, while a number of new intense peaks appear and at the same time their intensities increase with increasing pressure. These changes in the Raman spectrum, clearly seen at 20.7 GPa, unambiguously evidence the structural transition to a new high-pressure phase.

The Raman spectra (Fig. 2*b*) of the high-pressure phase, recorded upon pressure release, show a shift of the Raman peaks to lower energies, while the Raman intensity distribution does not change and the high-pressure phase is recovered at ambient conditions.

The pressure dependence of the phonon frequencies gives a better illustration of the effect of pressure on the $2D$-T polymer. This is shown in Fig. 3 for both phases [27]. The frequency of the majority of the peaks in the new phase can be traced back to the peaks of the initial $2D$-T polymer, which means that the C_{60} molecular cages are preserved up to the highest pressure of 27.5 GPa. There are specific characteristics in the pressure dependence of the phonon modes, which are indicative of $3D$ polymerization.

First, we see a strong sublinear pressure dependence of the $H_g(1)$ and $A_g(1)$ modes, which are related to radial out-of-plane displacements of the carbon atoms. This is associated with the fast decrease in the interlayer distance and therefore with the enhancement of the Van der Waals interaction among adjacent $2D$ polymeric layers. Such a behavior is typical for $2D$ polymeric layers and is observed in the $2D$-R polymer [30].

Second, the pressure coefficients $\partial\omega_i/\partial P$ of the Raman modes in the initial phase of the $2D$-T polymer, which vary between -1.2 and 7.6 cm^{-1}/GPa, are larger than those of the high-pressure phase, which are in the range from -0.2 to 4.1 cm^{-1}/GPa. For comparison, the pressure coefficients of the Raman modes in the pristine C_{60} vary between -4.1 and 9.8 cm^{-1}/GPa [31]. The above data are in accordance with the fact that polymerized materials become harder as the polymerization degree increases [8, 17, 32].

Third, several Raman modes, of the high-pressure phase, located in the frequency region 550–800 cm^{-1}, exhibit changes in their pressure slopes to higher values as the pressure decreases below 10 GPa. This behavior was predicted theoretically and is due to the increase in the tetragonal lattice parameter a of the high-pressure phase at ambient pressure by 0.3 Å, to the value 9.4 Å [17].

Fourth, an indication of the $3D$ polymerization is the behavior of the phonon mode at about 1040 cm^{-1}, which is related to the covalent intermolecular bonding within the $2D$ polymeric layers [8, 21]. This mode is associated with vibrations of sp^3-like coordinated carbon atoms; the frequency of this mode is lower than that of the T_{2g} mode of diamond [29] because of different lengths of sp^3-like bonds in the $2D$-T polymer (1.64 Å) and diamond (1.54 Å). The $3D$ polymeric phase proposed in [17] contains two types of sp^3-like coordinated carbon atoms with different bond lengths related to in-plane and out-of-plane covalent bonding. In the high-pressure phase, the 1040 cm^{-1} mode of the initial $2D$-T polymer splits into two components with frequencies 1029 and 1064 cm^{-1} due to the appearance of the out-of-plane covalent bonding, while the softening of the lower frequency band to 1029 cm^{-1} is related to the relaxation of the tetragonal lattice parameter [17]. In addition, the pressure coefficients of the Raman peaks at 1029 cm^{-1} (3.8 cm^{-1}/GPa) and 1064 cm^{-1} (2.8 cm^{-1}/GPa) are comparable to that of the T_{2g} mode of crystalline diamond (2.7 cm^{-1}/GPa) [33].

Finally, the changes in the region of the $A_g(2)$ PP mode are related to the breakdown of a large number of double C=C bonds in the high-pressure phase resulting in the disappearance of the PP mode and the appearance of a number of new Raman peaks, with the most intense of them located near 1842 cm^{-1}. The new Raman peaks in the region of the PP mode are related

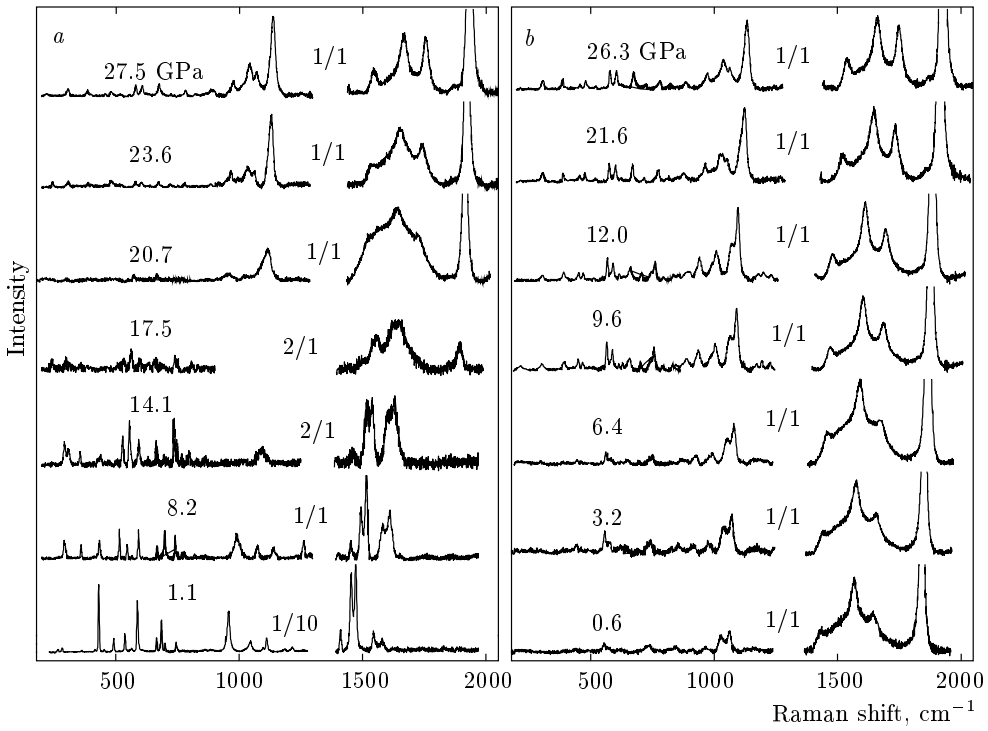

Fig. 2. Raman spectra of the $2D$-T polymer of C_{60} at 300 K and various pressures, recorded for (a) increasing and (b) decreasing pressure runs. The numbers m/n indicate the relative scale of the spectra

to stretching vibrations of the remaining double C=C bonds, which have different bond lengths [34].

The recovered high-pressure phase undergoes a violent transition, sort of being "detonated", after a period of a few days, probably due to the sample heating upon laser irradiation. The pieces of the detonated sample are characterized by two completely different Raman spectra shown in Figs. 4*c* and 4*d* [27]. The Raman spectrum of the main part of the detonated sample is similar to that recorded from a mixture of dimers and monomers of C_{60} (Fig. 4*c*) [2]. The presence of this phase in the detonated sample gives a definitive proof that the C_{60} molecular cages are preserved in the high-pressure phase of the $2D$-T polymer. The weak Raman spectrum of the other phase, which is only a small part of the detonated sample, is shown in Fig. 4*d*. The spectrum consists of two relatively broad peaks at 1342 and 1591 cm^{-1} and is similar to that of the D- and G-bands originating from microcrystalline graphite sample with defects [35].

The results of Raman measurements at high pressure have been verified by *in-situ* X-ray diffraction studies of the crystal structure of the $2D$-T at high pressure [36–38]. The behavior of the crystal lattice parameters of the planar $2D$-T and $2D$-R polymers of C_{60} at pressures up to 7 GPa was studied by X-ray diffraction in [37], but the crucial pressure range was not achieved. The structural characteristics inferred from high-pressure Raman data were verified by the X-ray study of the $2D$-T polymer at pressures up to 37 GPa, which has revealed a structural transition near 24 GPa [36]. As a result, the transformation from a $2D$ to a $3D$ polymer was clearly demonstrated. The obtained structural model, however, differs from that predicted theoretically [17] because the $3D$ polymerization was effected via the formation of interlayer $3+3$ cycloaddition along the body diagonal [36].

The compressibility of the initial $2D$-T polymer obtained by X-ray studies is highly anisotropic; the ambient-pressure compressibilities along and perpendicular to the polymeric layers differ by more than 20 times [36, 37]. After the transition to the high-pressure phase, the crystal structure remains tetragonal, the lattice parameter ratio c/a decreases abruptly from 1.66 to 1.36, while the anisotropy of compressibility disappears. The bulk modulus (407 GPa) of the high-pressure $3D$ polymeric phase determined by X-ray diffraction measurements [36] is considerably higher than that predicted theoretically [17] and slightly smaller than that of diamond (443 GPa). This is definitely a consequence

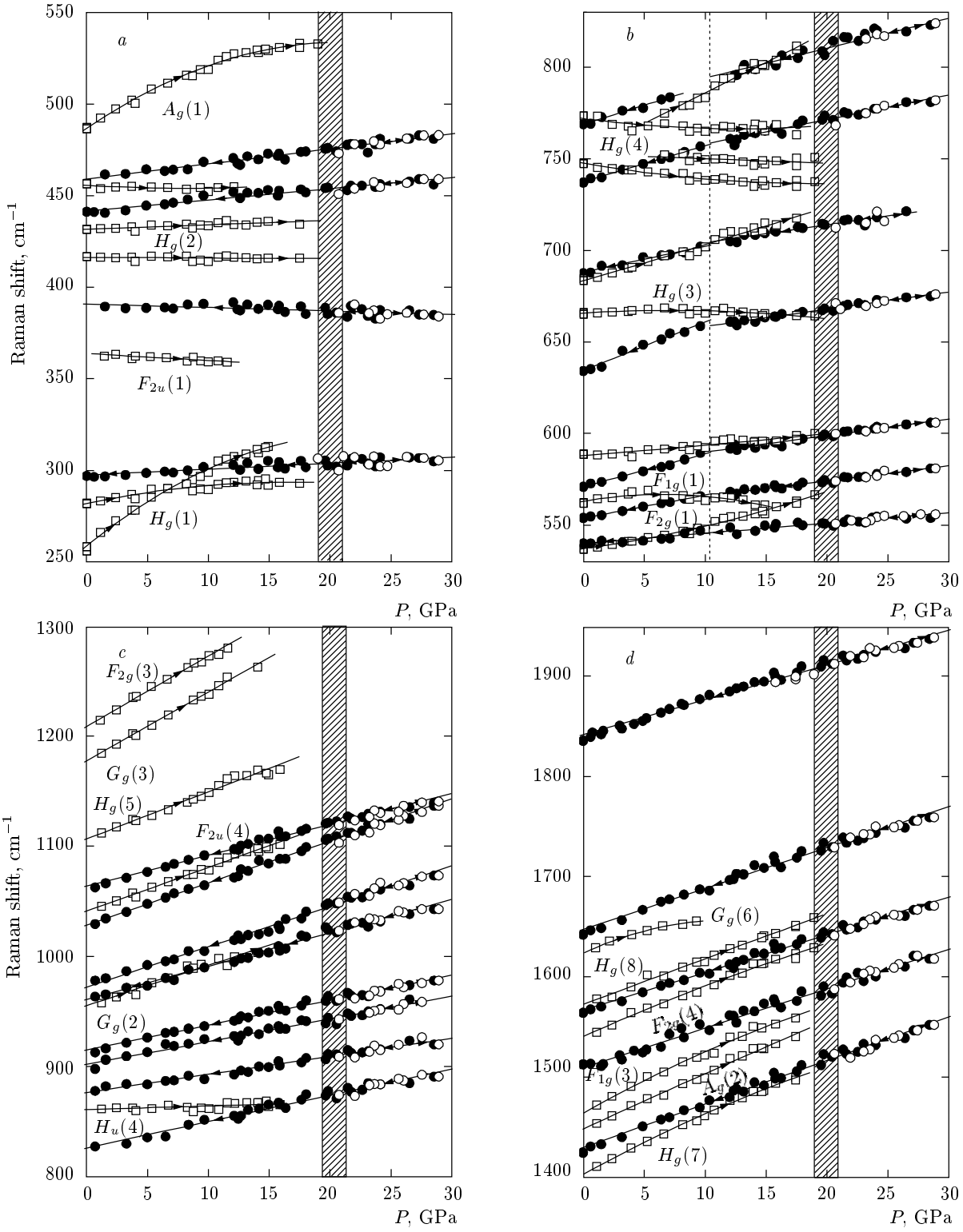

Fig. 3. Pressure dependence of the Raman modes of the $2D$-T polymer in the frequency ranges (a) 250–550 cm^{-1}, (b) 530–830 cm^{-1}, (c) 800–1300 cm^{-1}, and (d) 1400–1950 cm^{-1}. Squares and circles represent data respectively taken for the $2D$-T polymer in the initial and the high-pressure phase. The open (solid) symbols denote data taken for increasing (decreasing) pressure runs. Solid lines are guide to the eye, while arrows point to the pressure increase or decrease. The shaded area around 20 GPa shows the pressure range of the phase transformation

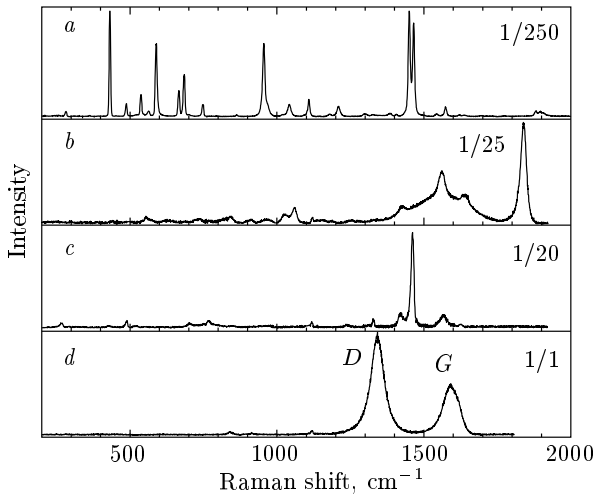

Fig. 4. Raman spectra of the initial $2D$-T polymer and of the recovered high-pressure phase after pressure release, recorded at ambient conditions. The numbers $1/n$ indicate the relative scale of the spectra. (a) The initial $2D$-T polymer. (b) The high-pressure phase of the $2D$-T polymer. (c) The main component among the pieces of the detonated sample identified as a mixture of the C_{60} monomer and the dimer. (d) The disordered graphite phase identified among the pieces of the detonated sample

of the obtained structural model of the $2D$-to-$3D$ transition [36], which differs from the one predicted theoretically in [17].

Thus, the X-ray diffraction study [36] confirms that the transformation found for the first time by Raman measurements [27, 28] is indeed of a structural nature and is related to $3D$ polymerization of the initial $2D$-T polymer. However, such a structural transition was not found in an earlier X-ray diffraction study of the $2D$-T polymer at high pressure [38], which has shown a gradual amorphization of the initial polymeric phase at pressures higher than 20 GPa. A possible reason for this disagreement is the strong dependence of the pressure-induced $3D$ polymerization of the $2D$-T polymer on the structural details of the initial polymeric phase.

As we have mentioned, there are two crystal structures of the $2D$-T polymer, characterized by the space groups $P\,4_2/mmc$ and $Immm$. Because the initial $2D$-T polymer in [36] was $Immm$ with an approximately 20 % impurity of $P\,4_2/mmc$, the $3D$ polymerization, which is characteristic of the $Immm$ structure, did occur. But in samples with a structure belonging to the $P\,4_2/mmc$ space group as the majority phase, a different transition is expected at a different pressure. Because this process competes with amorphization due to the nonhydrostaticity conditions in the diamond anvil cell, this can be the reason for the results observed in [38].

3. TRANSFORMATIONS OF THE $2D$-R POLYMER AT HIGH PRESSURE

To verify the theoretical predictions [20] about further polymerization of the linear and planar polymers of C_{60} under high pressure, a number of *in-situ* high-pressure Raman experiments were performed [30, 39, 40]. As in the case of the $2D$-T polymer, the $2D$-R polymer shows an irreversible transition at high pressure and room temperature to a new phase characterized by very broad Raman bands, typical of a disordered state [30]. A more detailed study by Raman spectroscopy, at pressures up to 30 GPa, have shown that the new high-pressure phase is most likely associated with a further $3D$ cross-linked polymerization at a pressure approximately 15 GPa via chaotic covalent bonding between adjacent polymeric layers [39].

The Raman spectra of the $2D$-R polymer of C_{60}, in the frequency range 100–2050 cm^{-1} recorded upon pressure increase up to 30 GPa are illustrated in Fig. 5*a* [39]. The initial spectrum, taken at about 0.9 GPa, is similar to that at ambient conditions, which exhibits typical Raman features of the $2D$-R polymer except some additional peaks, indicated by arrows, associated with the presence of oligomers in the starting material [21]. The frequencies and the assignment of the Raman modes of the $2D$-R polymer of C_{60}, in reference to irreducible representations of the C_{60} symmetry group, are tabulated in Table 2 [30]. The characteristics of the Raman spectra under high pressure are similar to those of other C_{60} polymers; the Raman peaks shift to higher energy, their bandwidth gradually increases, and intensity redistribution among various Raman modes occurs. The relative intensities of the $H_g(3)$, $H_g(4)$, $G_g(2)$, $F_{1g}(2)$, $H_g(8)$, and $G_g(6)$ modes increase and the intensities of the $H_g(1)$ and $A_g(1)$ modes decrease while the broadening of the Raman peaks is enhanced above 10 GPa. The Raman spectrum exhibits drastic changes near 15 GPa, where it becomes very diffuse and loses its fine structure in all frequency ranges. The transformation is preceded by a rapid decrease in the intensity of the $A_g(2)$ PP mode, which vanishes at pressures above 15 GPa. The broad Raman features above $P \geq 15$ GPa, designated as $\Omega(1)$–$\Omega(9)$ in Table 2, can be traced back to the initial $2D$-R polymer and seem to incorporate the cor-

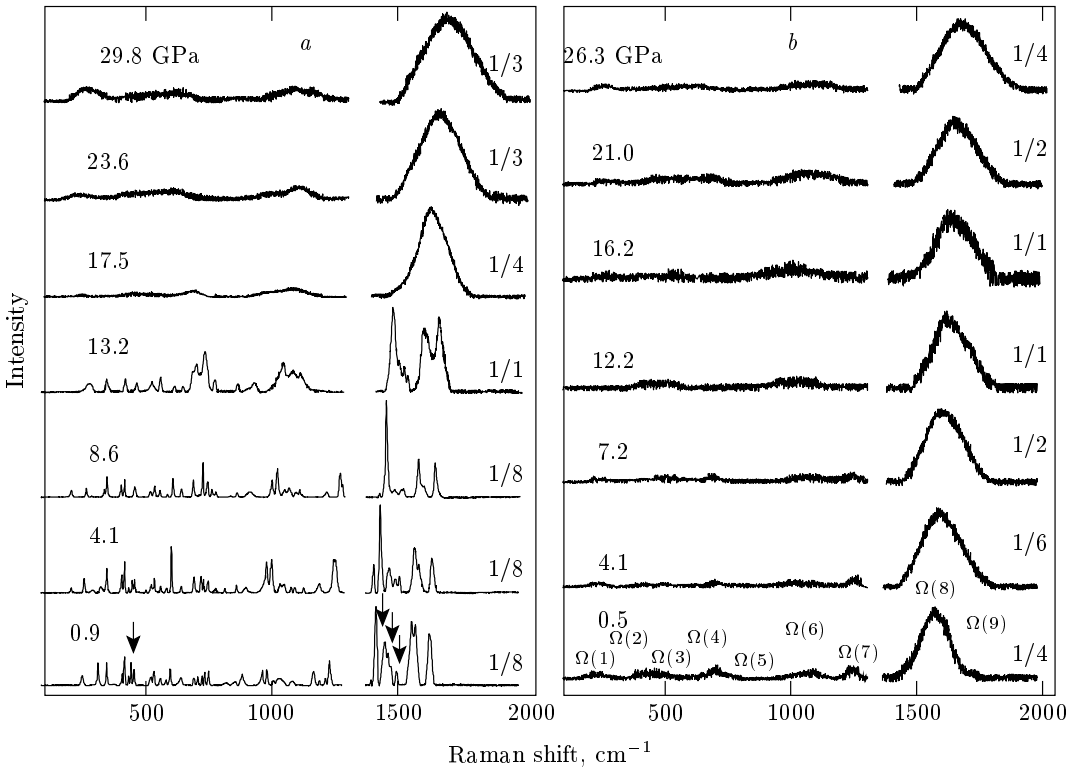

Fig. 5. Raman spectra of the $2D$-R polymer at room temperature and various pressures, recorded for (a) increasing and (b) decreasing pressure runs. The vertical arrows indicate peaks related to the presence of oligomers in the material. The numbers $1/n$ indicate the relative scale of the spectra

responding group of the narrow Raman peaks of this material.

Figure 5b shows the Raman spectra of the high-pressure phase upon pressure release [39]. Decreasing the pressure from 30 GPa to ambient pressure results in a gradual shift of the Raman peaks to lower energies without any observable changes in the Raman intensity distribution. The high-pressure phase remains stable down to ambient conditions and the recovered sample is rather stable at least for a period of about one week. The Raman spectra of the recovered material taken at various sites of the sample are identical and their diffuse nature is indicative of a highly disordered state. It is worth noting that the Raman spectrum of the recovered sample differs as much from that of the microcrystalline graphite with defects as from that of amorphous carbon [35].

The pressure dependences of the phonon frequencies of the $2D$-R polymer in the energy range 820–1720 cm^{-1} for the initial and the high-pressure phase are shown in Fig. 6. The Raman modes show a positive pressure shift with a linear dependence, which is reversible with pressure, at least up to 10 GPa, the highest pressure achieved in the first pressure run [30]. The shaded area around 15 GPa shows the pressure range of the irreversible phase transition to a new high-pressure phase. As can be seen from Fig. 6, the pressure dependences of the $\Omega(8)$ and $\Omega(9)$ modes in the downstroke pressure run are close to the pressure dependences of the corresponding group of modes $H_g(8)$ and $G_g(6)$ of the initial $2D$-R polymer located in this frequency range. The pressure coefficients of the Raman modes in the high-pressure phase vary between -1.4 and 4.7 cm^{-1}/GPa. They are smaller than those in the initial $2D$-R phase, ranging between -0.6 and 7.2 cm^{-1}/GPa, whereas the pressure coefficients in pristine C_{60} vary between -4.1 and 9.8 cm^{-1}/GPa [31]. The pressure dependences of the Raman modes strongly indicate that the $2D$-R polymer undergoes an irreversible transformation at a pressure near 15 GPa. The decrease in the intensity of the $A_g(2)$ mode and the enhancement of the neighboring $H_g(8)$ and $G_g(6)$ modes in the pre-transitional pressure region is reminiscent of an analogous behavior exhibited by these modes in the $2D$-T polymeric phase of C_{60} before its further polymerization under high pressure

Table 2. Phonon frequencies and pressure coefficients of the $2D$-R polymer of C_{60} and its high-pressure phase

$2D$-R polymer of C_{60}			High-pressure phase		
Mode	ω_i, cm^{-1}	$\partial\omega_i/\partial P$, cm^{-1}/GPa	Mode	ω_i, cm^{-1}	$\partial\omega_i/\partial P$, cm^{-1}/GPa
$H_g(1)$	245	2.3	$\Omega(1)$	228	1.3
$H_g(1)$	267	2.8			
$H_g(1)$	308	3.4			
$H_u(1)$	342	0.6			
$G_u(1)$	406	−0.4	$\Omega(2)$	397	3.1
$H_g(2)$	415	0.2			
$H_g(2)$	438	2.2			
$H_g(2)$	451	0.9			
$A_g(1)$	492	1.1	$\Omega(3)$	470	4.7
$F_{1u}(1)$	520	0.1			
$F_{2g}(1)$	532	0.3			
$F_{1g}(1)$	558	−0.2			
$H_u(2)$	579	0.8			
$H_u(2)$	596	1.4			
$H_u(3)$	640	0.4			
$H_g(3)$	695	−0.5	$\Omega(4)$	705	−0.8
$H_g(3)$	709	−0.6			
$F_{2u}(2)$	712	1.8			
$H_g(3)$	731	−0.2			
$H_g(4)$	749	−0.2			
$F_{2g}(2)$	749	1.8			
$H_g(4)$	767	0.4			
$H_g(4)$	776	0.3			
$F_{2u}(3)$	827	1.0			
$H_u(4)$	856	0.8			
$G_g(2)$	958	5.0	$\Omega(5)$	1025	−1.4
$F_{1g}(2)$	977	5.4			
$H_g(5)$	1078	3.9	$\Omega(6)$	1086	0.3
$H_g(5)$	1109	4.2			
$G_g(3)$	1158	7.2			
$H_g(6)$	1224	5.8			
$H_g(6)$	1230	6.2	$\Omega(7)$	1244	0.6
$H_g(7)$	1385	5.4			
$A_g(2)$	1410	5.6			
$F_{1g}(3)$	1495	3.5			
$H_g(8)$	1554	3.7			
$H_g(8)$	1563	3.9	$\Omega(8)$	1568	4.3
$H_g(8)$	1569	4.3			
$G_g(6)$	1621	3.6			
$G_g(6)$	1627	3.8	$\Omega(9)$	1638	3.3

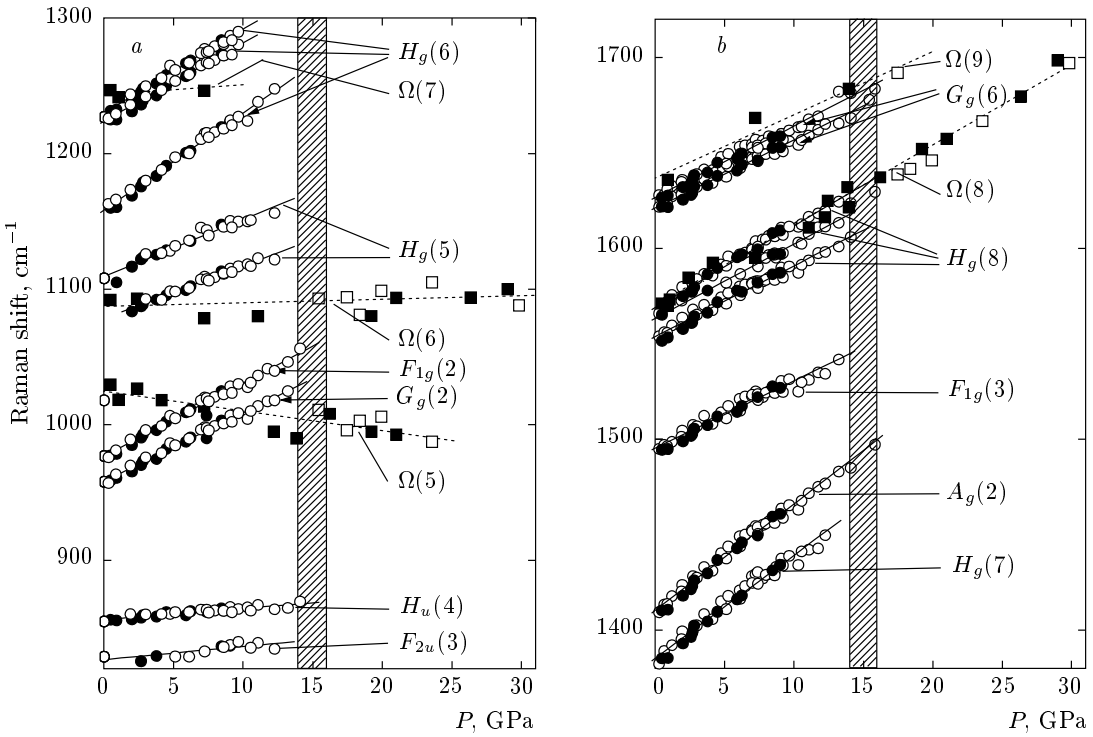

Fig. 6. The pressure dependence of the Raman modes of the $2D$-R polymer in the energy ranges (a) 820–1300 cm^{-1} and (b) 1380–1720 cm^{-1}. Circles (squares) represent data taken for the $2D$-R polymer in the initial phase (high-pressure phase). The open (solid) symbols denote data taken for increasing (decreasing) pressure runs. Solid lines are guides to eye. The shaded area around 15 GPa denotes the pressure range of the phase transformation

[27, 28]. In addition, the decrease in the pressure coefficients in the high-pressure phase is an indication of the $3D$ polymerization of the $2D$-R polymer, in accordance with the known experimental data and theoretical predictions that polymerized fullerenes become harder as the degree of polymerization increases [17, 20, 27, 28, 32, 36].

The application of high pressure to planar polymers of C_{60} preferentially decreases the distance between the polymeric layers due to the anisotropic compressibility of these materials. However, the creation of covalent bonds is possible only between the C atoms belonging to molecules of adjacent layers and having optimal relative orientations. The X-ray studies of the planar polymers of C_{60} at pressures up to 6 GPa have shown that the center-to-center distances of the nearest C_{60} cages between adjacent polymeric layers in the $2D$-R polymer decreases more rapidly than those in the $2D$-T polymer [37]. However, the relative molecular orientations and the atom-to-atom distances in the $2D$-T polymer are preferable for the formation of regular covalent bonds between molecules in adjacent polymeric layers [17, 27]. We can assume that the new bonds in the highly compressed $2D$-R polymer are randomly oriented due to nonoptimal molecular orientations. As a result, the new high-pressure polymeric phase exhibits a high degree of disorder due to random out-of-plane bond formation. This behavior differs from that of the $Immm$ body-centered pseudo-tetragonal crystal structure, which provides optimal relative orientations of C_{60} molecules and leads to the formation of regular out-of-plane covalent bonds manifested by narrow peaks in the Raman spectra of the high-pressure phase [17, 27, 28, 36, 41, 42]. We note that the inhomogeneity of the $2D$-T polymeric samples consisting of a mixture of the $Immm$ and $P\,4_2/mmc$ tetragonal phases can result in a spatially nonuniform Raman response of the high-pressure phase. The highly ordered high-pressure phase in the compressed $2D$-T polymer appears in a number of small islands that have the $Immm$ structure and are dispersed in the sample [28]. The rest of the sample has the $P\,4_2/mmc$ structure and is characterized by a rather diffuse Raman spectrum as well as by diffuse X-ray spectra of the high-pressure phase [38], somewhat reminiscent of the $2D$-R polymer of C_{60}.

Finally, the Raman spectrum of the high-pressure

phase does not show significant changes after annealing for a long time at temperatures below 500 K. However, the Raman spectrum of the annealed material at the temperature 550 K contains a relatively narrow and intense Raman band near 1464 cm^{-1}, related to the PP mode corresponding to the case of a mixture of monomers and dimers of C_{60} [39]. On the other hand, differential scanning calorimetry experiments clearly show the decomposition of linear and planar polymers of C_{60} in the temperature range near 530 K [43]. Thus, the behavior of the recovered high-pressure phase of the $2D$-R polymer is reminiscent of the other polymers of C_{60} and we can conclude that the C_{60} molecular cages are definitely preserved in the high-pressure phase. These results also show that the broadening of the Raman bands of the high-pressure phase has an intrinsic origin and they do not originate from pressure-induced imperfections and/or structural defects [39].

4. PRESSURE- AND PHOTO-INDUCED TRANSFORMATIONS IN THE LINEAR POLYMER OF C_{60}

In this section, we review the transformations of the $1D$-O polymer observed in Raman studies under high pressure and laser irradiation. In contrast to the pristine fullerene, the $2D$ polymers of C_{60} withstand laser irradiation, which does not cause their additional polymerization [2, 8]. The main effect of laser irradiation is the overheating of polymers within the laser beam spot at high laser intensities, which results in their decomposition. Among the polymers, the linear $1D$-O polymer is the most sensitive to laser irradiation, which may cause the photo-induced transformations manifested in its Raman spectra at a relatively small laser power density [44]. In addition, the application of high pressure to the $1D$-O polymer strongly enhances the rate of the photo-induced transformation, which occurs even at very low pressure and laser intensity [40, 45]. The linear $1D$-O polymer, in general, is less stable in comparison with the planar polymers of C_{60}. Its instability was also observed at increased temperature and pressure, namely at $T = 873$ K and $P = 2.5$ GPa; these conditions fall into the stability region of the $2D$-T polymer in the pressure–temperature phase diagram of C_{60} [8, 46]. The X-ray diffraction and Raman studies of the linear $1D$-O polymer annealed under these temperature/pressure conditions have shown its gradual transformation to the $2D$-T polymeric phase. A detailed investigation of the samples annealed under various time intervals has revealed that the transformation proceeds via the intermediate dimer state (D) in a two-stage process, from the linear $1D$-O polymer to dimer D and then from dimer D to the planar $2D$-T polymer [46].

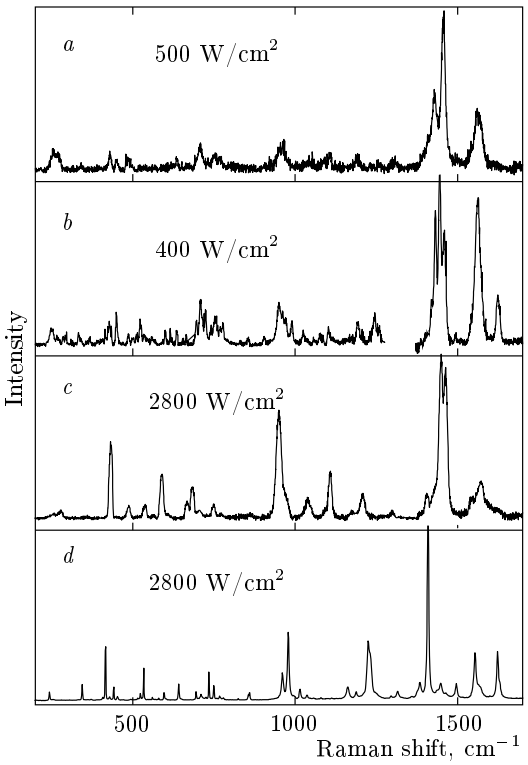

Fig. 7. Raman spectra of (a) the initial $1D$-O polymer at normal conditions and (b) the transformed $1D$-O polymer at 0.3 GPa recorded with different excitation power densities. Raman spectra of (c) $2D$-T and (d) $2D$-R at ambient conditions are shown for comparison

The Raman spectra of the $1D$-O polymer under high pressure and room temperature show that the material transformation occurrs at any initial pressure upon loading the diamond anvil cell (see Fig. 7) [40]. Figure 7a shows the Raman spectrum of the pristine $1D$-O polymer recorded at ambient conditions and Fig. 7b shows the Raman spectrum recorded in the first pressure run with the starting pressure about 0.3 GPa [40]. This spectrum has quite a different structure: the majority of bands are split and the number of peaks is increased. The same behavior is observed for other pressure runs at any starting pressure, even as small as 0.1 GPa. The observed pressure-driven transformation is not typical: it is impossible to find the threshold pressure using the diamond anvil cell because of the small pressure resolution. For comparison, Figs. 7c and 7d show the Raman spectra of the planar

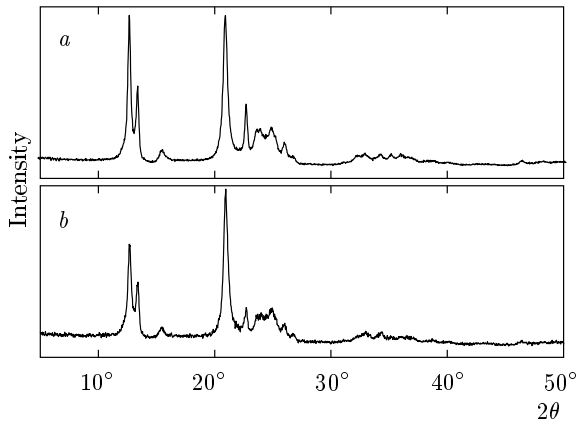

Fig. 8. X-ray diffraction pattern at normal conditions of (*a*) the initial orthorhombic phase of C_{60} and (*b*) the pressure-treated $1D$-O polymer after pressure release

$2D$-T and $2D$-R polymeric phases of C_{60}, which differ significantly in the number, position, and relative intensities of the peaks from that of the transformed $1D$-O polymer.

It is important to note that the comparison of the X-ray diffraction pattern of the initial $1D$-O polymer at normal conditions with that of the $1D$-O polymer treated at 3 GPa has not revealed any difference between them after pressure release. These data, shown in Fig. 8, are practically identical; the positions of all peaks are the same, while small differences in peak intensities can be related to the powder material preparation [40]. On the other hand, the *ex-situ* Raman spectrum of the pressure-treated $1D$-O polymer, taken after pressure release, is the same as the spectrum of the initial polymer. At the same time, the transformation is clearly observed in the *in-situ* high-pressure Raman study, which implies the crucial role of laser irradiation in this pressure-driven transition [40, 45].

The stability of the $1D$-O polymer under laser irradiation at ambient conditions was also studied at various laser power densities (Fig. 9) [44]. The Raman spectra taken at laser power densities up to 1280 W/cm^2 (Figs. 9*a* and 9*b*) do not show any changes within the time scale of the experiment. However, a new Raman band appears near 1446 cm^{-1} in the Raman spectrum at the laser power density 3200 W/cm^2. Further increase of the laser power density leads to the enhancement of the new band; at the highest laser power density of 25600 W/cm^2 (Fig. 9*d*), the Raman spectrum is reminiscent of that of the photo-transformed $1D$-O polymer taken at $P = 0.1$ GPa and a laser power density of 400 W/cm^2 (Fig. 9*e*) [44].

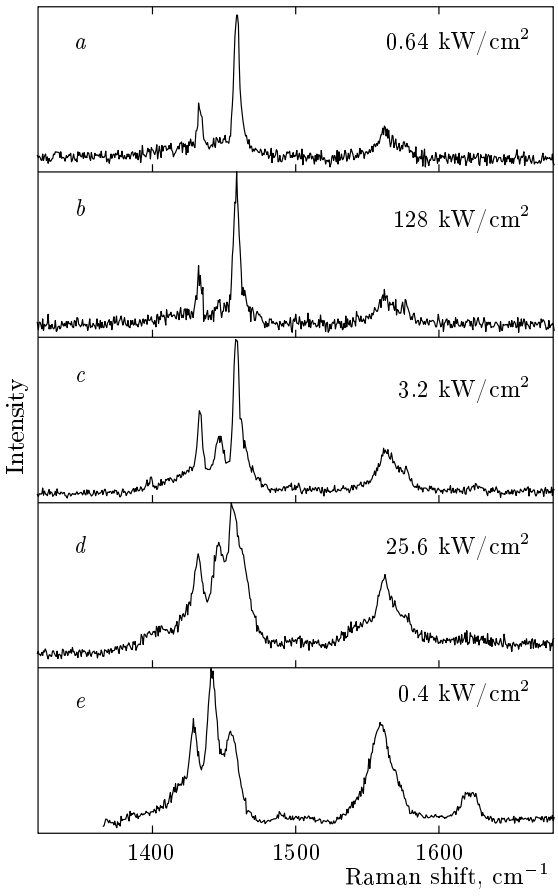

Fig. 9. Raman spectra of the pristine $1D$-O polymer recorded at ambient conditions and various excitation power densities of the 514.5-nm Ar^+ laser line (panels *a*–*d*). The spectrum of the transformed $1D$-O polymer at 0.1 GPa is also included (*e*)

We note that the photo-induced polymerization of the $1D$-O polymer occurs at the laser power density approximately equal to 3200 W/cm^2, a value that considerably exceeds the value 5 W/cm^2 reported for the photo-polymerization of the monomer C_{60} [2].

The application of high pressure enhances the process, resulting in an essential increase in the photo-polymerization rate and in the reduction of the laser power density inducing the transformation. The C_{60} molecules in the ground state cannot take part in the [2+2] cycloaddition reaction due to the Woodward–Hoffmann rule, which states that the coupling of the C_{60} molecules in their ground state is not favorable due to symmetry limitations [47]. But the molecular orbital of the excited state of C_{60}, being populated by light absorption, has a symmetry favorable for the dimer formation. The formation of dimers at high pressure

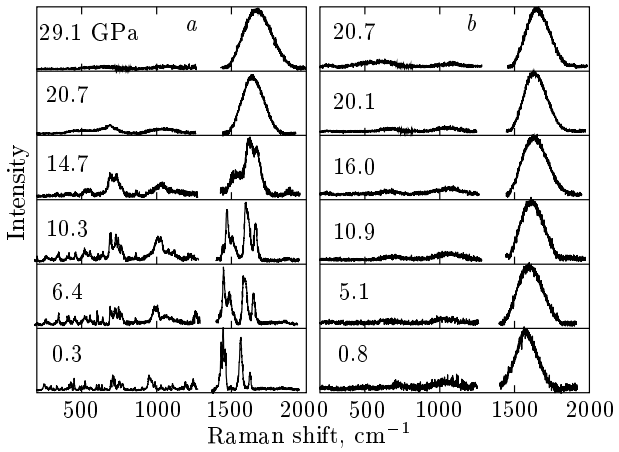

Fig. 10. Raman spectra of the photo-transformed $1D$-O polymer of C_{60} at room temperature and various pressures, recorded upon (a) pressure increase and (b) pressure decrease

occurs without light irradiation [48] because the pair interaction at high pressure is out of symmetry limitations. Hence, the simultaneous effect of pressure and light irradiation stimulates the polymerization process, which results in a considerable increase in the polymerization rate.

The structural aspects of the observed pressure-enhanced photo-assisted transition were studied by *in-situ* X-ray powder diffraction measurements at high pressure using the diamond anvil cell; the results clearly show the transformation of the $1D$-O polymer to a new phase at a starting pressure of 0.2 GPa [49]. The pressure-driven transformation initiated by X-ray irradiation is due to the conjunction of adjacent linear polymeric chains of the $1D$-O polymer [49]. Unfortunately, this study has not revealed the detailed structure of the new polymeric phase because the low-resolution diffraction profiles along with the small number of peaks did not permit further refinement.

The photo-transformed $1D$-O polymer is not structurally stable upon pressure application, as Raman measurements at pressures up to 29 GPa have shown [50, 51]. Significant changes were observed near 15 GPa, where the Raman spectrum loses its fine structure in all frequency regions and becomes very diffuse. This transformation was preceded by a rapid decrease in the intensity of the peaks related to the $A_g(2)$ mode of the pristine C_{60} accompanied by a relative increase in the intensities of the $H_g(8)$ and $G_g(6)$ modes. The broad Raman features in the spectrum of the high-pressure phase above 15 GPa can be traced back to the photo-transformed $1D$-O polymer of C_{60} and seem to incorporate the corresponding group of the broad Raman bands of this phase. They are typical of a disordered phase; the peaks shift to lower energies upon pressure decrease, without any observable changes in their intensity distribution (Fig. 10b). The high-pressure phase is recovered at normal conditions and remains stable at least for several hours.

The pressure dependence of the Raman mode frequencies of the photo-transformed $1D$-O polymer of C_{60} in the energy ranges 240–790 cm^{-1} and 860–1720 cm^{-1} is shown in Fig. 11. All changes in the pressure dependence of all Raman modes are reversible with pressure if the pressure does not exceed 12 GPa. The pressure coefficients of some Raman bands change abruptly near 4 GPa. The slopes of the low-energy Raman modes at 288 cm^{-1} and 333 cm^{-1} respectively change from 8.4 cm^{-1}/GPa to 2.2 cm^{-1}/GPa and from 2.7 cm^{-1}/GPa to 0.04 cm^{-1}/GPa. For the high-frequency modes at 1429 cm^{-1} and 1442 cm^{-1}, the respective pressure coefficients change from 3.2 cm^{-1}/GPa to 6.2 cm^{-1}/GPa and from 7.0 cm^{-1}/GPa to 4.0 cm^{-1}/GPa. In addition, the band at 1559 cm^{-1} splits near 4 GPa and the pressure coefficients of the split components are slightly different: 4.9 cm^{-1}/GPa and 4.5 cm^{-1}/GPa for the higher and lower-energy component, respectively. The peculiarities near 4 GPa can be an indication of a reversible structural phase transition possibly related to minor changes in the packing of the conjugated linear polymeric chains. However, a high-pressure X-ray powder diffraction study [49] has not revealed clear changes in the diffraction patterns near 4 GPa. This can be related to the low resolution of the data and to a small number of peaks, which did not permit the complete refinement of the structure in [49].

The changes in the Raman spectra near 15 GPa are apparently related to an irreversible transformation. More specifically, the rapid disappearance of the PP mode in the pre-transitional pressure range, the drastic broadening of Raman bands, and the behavior upon pressure release provide unambiguous evidence of an irreversible transformation to a highly disordered state [50]. This behavior is reminiscent of the analogous behavior of the $2D$-R polymer of C_{60} before its further polymerization under high pressure [30]. As in the case of the $2D$-R polymer, the new bonds can be formed in a random way due to some distortion in the molecular orientations. As a result, the new high-pressure phase exhibits a high degree of disorder characterized by random polymerization.

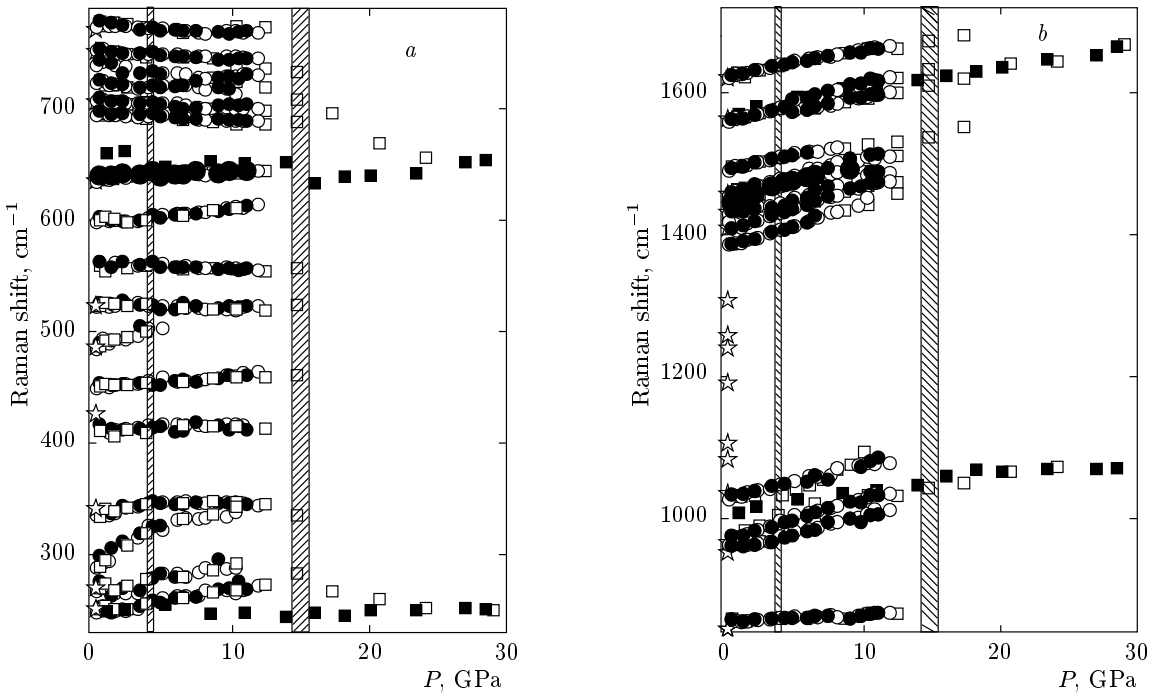

Fig. 11. Pressure dependence of the Raman frequencies of the photo-transformed $1D$-O polymer of C_{60} in the ranges (a) 240–790 cm^{-1} and (b) 860–1720 cm^{-1}. Circles and squares represent data respectively taken upon two different pressure runs up to 12 and 29 GPa. Stars denote the Raman frequencies of the initial $1D$-O polymer at normal conditions. The open (solid) symbols represent data recorded upon pressure increase (decrease). Shaded areas around 4 and 15 GPa mark pressure values where changes in the pressure dependence were observed

The recovered sample was tested by means of micro-Raman probing in order to check its stability at ambient conditions. The high-pressure phase is metastable; it transforms without heating rather quickly to a phase that demonstrates Raman features resembling those of the initial $1D$-O polymer of C_{60}. But a detailed analysis of the peak positions shows that the final material is a mixture of the monomer and the dimer of C_{60} [50, 51]. The behavior of the recovered high-pressure phase of the photo-transformed $1D$-O polymer differs from that of the high-pressure phase of the $2D$-R polymer, which is more stable and transforms into a mixture of pristine and dimerized C_{60} only under sample annealing [30].

5. THERMAL STABILITY OF FULLERENE POLYMERS

The high-pressure phases of the planar and linear polymers of C_{60} are metastable and transform under heating to a mixture of dimer and monomer forms of C_{60}, as we have seen in the preceding sections. The initial linear and planar polymers of fullerene are also very sensitive to heating; their stability at increased temperatures was studied by differential scanning calorimetry, X-ray diffraction, and Raman and IR spectroscopy [43, 52–55]. These studies have revealed that the heating to 560 K results in the destruction of intermolecular C–C bonds and reversion to the initial C_{60} monomer phase. The differential scanning calorimetry performed in various polymeric phases with a heating rate of 10–20 K/min show a strong endothermic peak between 525 and 565 K, which was not observed during the cooling scan. The transition temperature depends on the polymeric phase and somewhat on the scanning rate, indicating that the polymer decomposition process is controlled by kinetics.

The change of enthalpy related to the complete decomposition of polymers is the highest for the C_{60} dimers, its value decreases for linear polymeric chains and becomes smallest for the planar polymeric phases [43]. Therefore, the free energy of the monomer state is higher than the free energies of polymeric phases. The stability of the C_{60} monomer at ambient conditions is due to the energy barrier that separates polymeric states from the monomer state [43]. The appearance of this barrier is related to a considerable

deformation, up to 5 % in diameter [8], of the fullerene molecular cage in polymeric phases. The energy barrier for the $2D$-R polymer, obtained from the X-ray thermal expansion measurements [52], is 1.9 ± 0.2 eV/molecule, whereas the calculated values are 1.6 eV/molecule [56] and 1.7 eV/molecule [57].

The differences in the enthalpy change between the various polymeric phases and the kinetics of polymer decomposition suggest that the process of the temperature-induced decomposition of polymeric fullerene networks possibly involves formation of intermediate polymeric/oligomeric states. Studies of the intermediate states can be based on the distinct difference of the Raman frequencies of the PP mode for various polymeric/oligomeric phases, which allows their identification during the decomposition process. The intermediate states formed during the decomposition of the $2D$-R polymer of C_{60} were studied by spatially resolved Raman spectroscopy; the Raman spectra of a number of small pieces of polymers were measured after their treatment at various temperatures up to 600 K [55, 58].

Raman spectra of the $2D$-R polymer measured in the region of the $A_g(2)$ mode, after sample treatment for 0.5 h at various temperatures, shown in Fig. 12 [58], do not manifest any detectable changes up to the treatment temperature 510 K, while at higher temperatures, the Raman spectra change significantly. The material transformation proceeds through an intermediate state; the Raman spectrum of the material treated at 523 K shows weak peaks typical of the PP mode of the $2D$-T and the $1D$-O polymer as well as of the C_{60} dimers and monomers that coexist with the PP mode of the initial $2D$-R polymer. Inclusion of $2D$-T-like oligomers in the intermediate state can be deduced from the Raman line at approximately 1447 cm^{-1}, characteristic of the PP mode in the $2D$-T polymer, while the Raman peak near 1459 cm^{-1} suggests the presence of linear polymeric chains.

The kinetics of the $2D$-R polymer decomposition was studied, after the sample treatment at 513 K, for a duration between 0.5 and 2.0 h. Raman spectra in the region of the $A_g(2)$ PP mode indicate that the mode intensity gradually decreases as the annealing time increases, whereas the intensity of the peaks associated with the presence of the $2D$-T- and the $1D$-O-like oligomers as well as with the monomeric C_{60} gradually increases. The treatment for 2 h leads to the complete decomposition of the $2D$-R polymer because the $A_g(2)$ mode peak attributed to the C_{60} monomer dominates the Raman spectrum. Figure 13 shows the intensity of the $A_g(2)$ mode of the $2D$-R polymer normalized to the sum of the corresponding peaks associated with all polymeric/oligomeric phases of C_{60} as a function of the treatment time for different temperatures [58]. We can estimate the barrier between the $2D$-R polymer and monomer states because the polymer decomposition time as a function of the treatment temperature obeys the Arrhenius equation

$$\tau(T) = A \exp(E_A/k_B T),$$

where E_A is the activation energy (in fact, the energy barrier between the polymer and monomer states), k_B is the Boltzmann constant, T is the treatment temperature, and $\tau(T)$ is the temperature-dependent polymer decomposition time constant, while the constant A measured in time units is related to the characteristic phonon frequency (the inset in Fig. 13). The experimental value of the activation en-

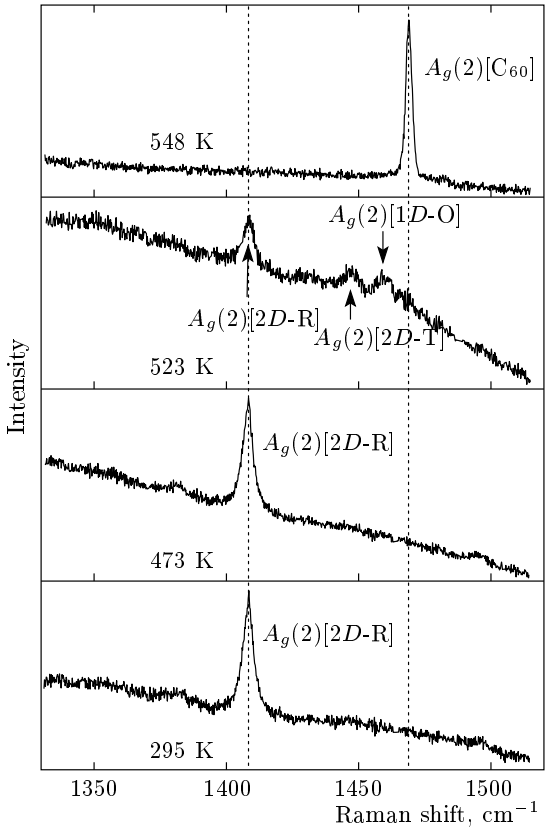

Fig. 12. Raman spectra of the $2D$-R polymer measured at room temperature in the frequency region of the $A_g(2)$ mode (left vertical line) after high-temperature treatment for 0.5 h at various temperatures. The arrows mark PP modes related to oligomers in a partially decomposed intermediate state. After the complete decomposition at 548 K, only the PP mode of monomer C_{60} remains in the spectrum (right vertical line)

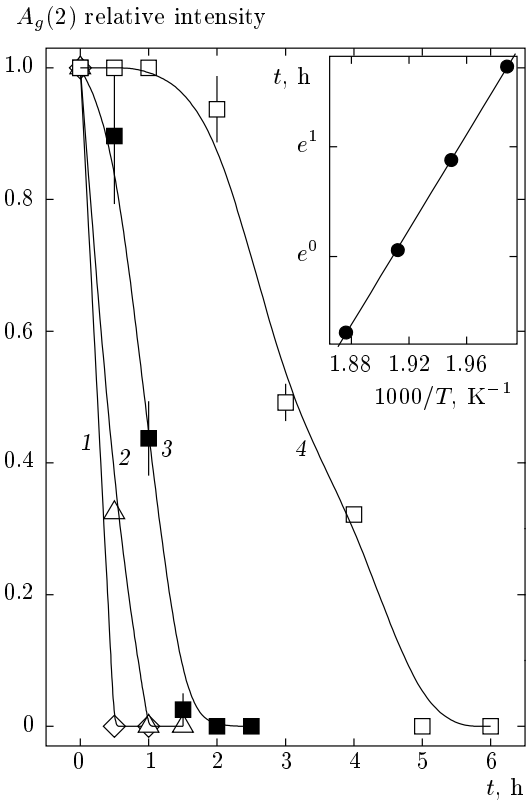

Fig. 13. Intensity of the $A_g(2)$ peak of the initial $2D$-R polymer normalized to the sum of the $A_g(2)$ peaks associated with the $2D$-R polymer, $2D$-T-like, and $1D$-O-like oligomers as well as with the monomer/dimer mixture of C_{60}, as a function of the heat treatment time at temperatures 533 K (*1*), 523 K (*2*), 513 K (*3*), and 503 K (*4*). The data were averaged over different samples and the error bars refer to the standard error of the mean, while the lines are guides to the eye. Inset: Arrhenius plot of the polymer complete decomposition time versus the treatment temperature

ergy $E_A = 1.76 \pm 0.07$ eV/molecule obtained in [58] is in good agreement with theoretical calculations [57, 58]. It is interesting that the estimations of the complete decomposition time of the $2D$-R polymer from the above data gives 450 million years at normal conditions, but it collapses to 62 h at $T = 473$ K. Thus, the fullerene polymers demonstrate rather large fragility at increased temperatures, which may be a reason limiting their prospects for practical use.

6. CONCLUSIONS

The $2D$-T polymer of C_{60} undergoes an irreversible phase transition near 20 GPa. The prominent Raman peaks related to the fullerene cage and the irreversibility of the high-pressure phase support the assumption of an ordered $3D$ cross-linked structure. The X-ray study of the $2D$-T polymer at high pressure confirms the transition near 24 GPa associated with the formation of interlayer $3+3$ cycloaddition along the body diagonal. The high-pressure $3D$ polymeric phase demonstrates high hardness; the bulk modulus determined from X-ray data is 407 GPa, which is slightly smaller than that of diamond (443 GPa).

The $2D$-R polymer of C_{60} under high pressure undergoes an irreversible transformation at $P \approx 15$ GPa. The diffuse Raman spectrum of the high-pressure phase is typical of a disordered phase. The high-pressure phase is formed in the $2D$-R polymer, most likely, by random creation of covalent bonds between adjacent polymeric layers due to the various distortions in molecular orientations.

The linear $1D$-O polymer of C_{60} is sensitive to laser irradiation and transforms into a new polymeric phase under irradiation at laser power densities two orders of magnitude higher than that needed for the polymerization of the C_{60} monomer. The photo-polymerization rate drastically increases under pressure and the transformation becomes almost instantaneous. The structure of the pressure-enhanced photo-induced $1D$-O polymer is associated with the conjugation of the adjacent polymeric chains. The photo-transformed $1D$-O polymer of C_{60} shows further polymerization at about 15 GPa to a $3D$ cross-linked disordered phase characterized by diffuse Raman spectra.

The high-pressure phases of linear and planar crystalline polymers of C_{60} recovered to ambient conditions are metastable and transform under heating into a mixture of pristine and dimerized C_{60}. This behavior is similar to the behavior of other polymeric fullerene states, which decompose near 535 K. The estimated complete decomposition time of the $2D$-R polymer is 450 million years at normal conditions, whereas it collapses to 62 h at 473 K. The fullerene polymers demonstrate rather large fragility at increased temperatures.

Support of the RFBR (Russia) and the General Secretariat for Research and Technology (Greece) is gratefully acknowledged. The authors thank Drs. J. Arvanitidis, D. Christofilos, K. Papagelis, S. Assimopoulos, A. Soldatov, T. Wägberg, S. Yamanaka, V. Davydov, and V. Agafonov for their help with the preparation and characterization of various polymers of C_{60}, and Profs. Y. Iwasa, B. Sundqvist, K. Prassides, and S. Ves for the helpful collaboration.

REFERENCES

1. H. W. Kroto, J. R. Heath, S. C. O'Brien et al., Nature **318**, 162 (1985).
2. A. M. Rao, P. Zhou, K.-A. Wang et al., Science **259**, 955 (1993).
3. J. Winter and H. Kuzmany, Sol. St. Comm. **84**, 935 (1992).
4. P. W. Stephens, G. Bortel, G. Faigel et al., Nature **370**, 636 (1994).
5. Y. Iwasa, T. Arima, R. M. Fleming et al., Science **264**, 1570 (1994).
6. I. O. Bashkin, V. I. Rashupkin, A. F. Gurov et al., J. Phys.: Condens. Matter **6**, 7491 (1994).
7. M. Nunẽz-Regueiro, L. Marques, J.-L. Hodeau et al., Phys. Rev. Lett. **74**, 278 (1995).
8. B. Sundqvist, Adv. in Phys. **48**, 1 (1999).
9. V. V. Brazhkin, A. G. Lyapin, and S. V. Popova, Pis'ma v Zh. Eksp. Teor. Fiz. **64**, 775 (1996).
10. V. Blank, M. Popov, S. Buga et al., Phys. Lett. A **188**, 281 (1994).
11. V. D. Blank, S. G. Buga, G. A. Dubitsky et al., Carbon **36**, 319 (1998).
12. L. Marques, M. Mezouar, J.-L. Hodeau et al., Science **283**, 1720 (1999).
13. L. A. Chernozatonskii, N. R. Serebryanaya, and B. N. Mavrin, Chem. Phys. Lett. **316**, 199 (2000).
14. R. Moret, Acta Cryst. A **61**, 62 (2005).
15. A. V. Dzyabchenko, V. Agafonov, and V. A. Davydov, Crystallogr. Rep. **44**, 18 (1999).
16. R. S. Ruoff and A. L. Ruoff, Nature **350**, 663 (1991).
17. S. Okada, S. Saito, and A. Oshiyama, Phys. Rev. Lett. **83**, 1986 (1999).
18. S. Okada and S. Saito, Phys. Rev. B **59**, 1930 (1999).
19. S. Saito and A. Oshiyama, Phys. Rev. Lett. **66**, 2637 (1991).
20. E. Burgos, E. Halac, R. Weht et al., Phys. Rev. Lett. **85**, 2328 (2000).
21. V. A. Davydov, L. S. Kashevarova, A. V. Rakhmanina et al., Phys. Rev. B **61**, 11936 (2000).
22. J. Arvanitidis, K. Papagelis, K. P. Meletov et al., Phys. Rev. B **59**, 3180 (1999).
23. G. A. Kourouklis, S. Ves, and K. P. Meletov, Physica B **265**, 214 (1999).
24. V. A. Davydov, L. S. Kashevarova, A. V. Rakhmanina et al., Phys. Rev. B **58**, 14786 (1998).
25. J. Winter, H. Kuzmany, A. Soldatov et al., Phys. Rev. B **54**, 17486 (1996).
26. J. Arvanitidis, K. P. Meletov, K. Papagelis et al., J. Chem. Phys. **114**, 9099 (2001).
27. K. P. Meletov, J. Arvanitidis, I. Tsilika et al., Phys. Rev. B **63**, 054106 (2001).
28. K. P. Meletov, I. Tsilika, S. Assimopoulos et al., Chem. Phys. Lett. **341**, 435 (2001).
29. S. A. Solin and A. K. Ramdas, Phys. Rev. B **1**, 1687 (1970).
30. K. P. Meletov, J. Arvanitidis, G. A. Kourouklis et al., Chem. Phys. Lett. **357**, 307 (2002).
31. K. P. Meletov, D. Christofilos, S. Ves, and G. A. Kourouklis, Phys. Rev. B **52**, 10090 (1995).
32. J. Haines and J. M. Leger, Sol. St. Comm. **90**, 361 (1994).
33. A. F. Goncharov, I. N. Makarenko, and S. M. Stishov, Pis'ma v Zh. Eksp. Teor. Fiz. **41**, 150 (1985).
34. D. A. Long, *Raman Spectroscopy*, McGraw-Hill, London (1976), p. 158.
35. R. J. Nemanich and S. A. Solin, Phys. Rev. B **20**, 392 (1979).
36. Dam Hieu Chi, Y. Iwasa, T. Takano et al., Phys. Rev. B **68**, 153402 (2003).
37. S. Kawasaki, A. Yao, Y. Matsuoka et al., Sol. St. Comm. **125**, 637 (2003).
38. J. M. Leger, J. Haines, V. A. Davydov, and V. Agafonov, Sol. St. Comm. **121**, 241 (2002).
39. K. P. Meletov, G. A. Kourouklis, J. Arvanitidis et al., Phys. Rev. B **68**, 094103 (2003).
40. K. P. Meletov, V. A. Davydov, A. V. Rakhmanina et al., Chem. Phys. Lett. **416**, 220 (2005).
41. K. P. Meletov, J. Arvanitidis, S. Assimopoulos et al., Zh. Eksp. Teor. Fiz. **122**, 849 (2002).
42. G. A. Kourouklis and K. P. Meletov, New Diamond and Frontier Carbon Techn. **12**, 303 (2002).
43. Y. Iwasa, K. Tanoue, T. Mitani, and T. Yagi, Phys. Rev. B **58**, 16374 (1998).

44. K. P. Meletov, V. A. Davydov, A. V. Rakhmanina et al., Chem. Phys. Lett. **428**, 298 (2006).

45. K. P. Meletov, V. A. Davydov, A. V. Rakhmanina, and G. A. Kourouklis, Fullerenes, Nanotubes, and Carbon Nanostr. **14**, 421 (2006).

46. T. Wagberg, A. Soldatov, and B. Sundqvist, Eur. Phys. J. B **49**, 59 (2006).

47. J. Fagerstrom and S. Stafstrom, Phys. Rev. B **53**, 13150 (1996).

48. V. A. Davydov, L. S. Kashevarova, A. V. Rakhmanina et al., Pis'ma v Zh. Eksp. Teor. Fiz. **68**, 881 (1998).

49. R. Le Parc, C. Levelut, J. Haines et al., Chem. Phys. Lett. **438**, 63 (2007).

50. K. P. Meletov and G. A. Kourouklis, Chem. Phys. Lett. **443**, 127 (2007).

51. K. P. Meletov, V. A. Davydov, J. Arvanitidis et al., Zh. Eksp. Teor. Fiz. **134**, 726 (2008).

52. P. Nagel, V. Pasler, S. Lebedkin et al., Phys. Rev. B **60**, 16920 (1999).

53. M. V. Korobov, V. M. Senyavin, A. G. Bogachev et al., Chem. Phys. Lett. **381**, 410 (2003).

54. M. V. Korobov, A. G. Bogachev, A. A. Popov et al., Carbon **43**, 954 (2005).

55. K. P. Meletov, J. Arvanitidis, D. Christofilos et al., Fullerenes, Nanotubes, and Carbon Nanostr. **18**, 396 (2010).

56. C. Hui and G. E. Scuseria, Phys. Rev. Lett. **74**, 274 (1995).

57. S. Saito and S. Okada, AIP Conf. Proc. **442**, 198 (1998).

58. K. P. Meletov, J. Arvanitidis, D. Christofilos et al., Carbon **48**, 2974 (2010).